Water Practice & Technology

IWA PUBLISHING

Water Practice & Technology Vol 18 No 9, 2045 doi: 10.2166/wpt.2023.139

The role of metallic nickel nanoparticles to remove dispersed oil from produced water in Sudan oil field plant

M. S. Suliman[a], Sahl Yasin [b,*] and Abdelhafeez M. A. Mohammed[c,d]

[a] Petroenergy E&P Co., Ltd., Khartoum, Sudan
[b] Sudanese Chemical Society, Khartoum, Sudan
[c] Department of Chemistry, College of Science & Arts, King Abdulaziz University, P.O. Box 344, Rabigh 21911, Saudi Arabia
[d] Department of Chemistry, Alzaiem Alazhari University, P.O. Box 1432, Khartoum North 13311, Sudan
*Corresponding author. E-mail: sahlyasin@hotmail.com

SY, 0000-0002-6355-1622

ABSTRACT

In this study, nickel nanoparticles (NiNPs) were synthesized and utilized for removing dispersed oil from oilfield-produced water in Sudan. The synthesis process involved using two concentration of hydrazine as a reducing agent and sodium hydroxide as solvent. Physiochemical characterizations, such as X-ray diffraction (XRD) and transmission electron microscopy (TEM), confirmed the successful preparation of NiNPs. The TEM analysis revealed an average particle size ranging from 70 to 90 nm, with a change in morphology from star-shaped to monodispersed spherical particles. The crystal structure analysis confirmed the face-centered-cubic (FCC) configuration of the NiNPs, validating their structural properties. Significantly, the NiNPs demonstrated an impressive capability to remove oil form produced water, achieving a remarkable efficiency of 98% in eliminating dispersed oil from produced water. The oil removal process followed Freundlich isotherms, as evidenced by the high value of the linear regression coefficient. Additionally, the kinetics of the oil removal process conformed well to the pseudo-second-order model, indicating a rapid reaction. This study successfully demonstrated the efficient removal of dispersed oil from produced water using nickel nanoparticles, which interacted physically with the oil particles. These findings highlight the potential of NiNPs as an effective adsorbent for treating oilfield-produced water and mitigating environmental contamination.

Key words: dispersed oil, nickel nanoparticles, Sudan oilfields

HIGHLIGHTS

- Nickel has been synthesized by two different concentrations of hydrazine.
- This is the first time testing metallic nickel nanoparticles for this purpose in Sudan.

GRAPHICAL ABSTRACT

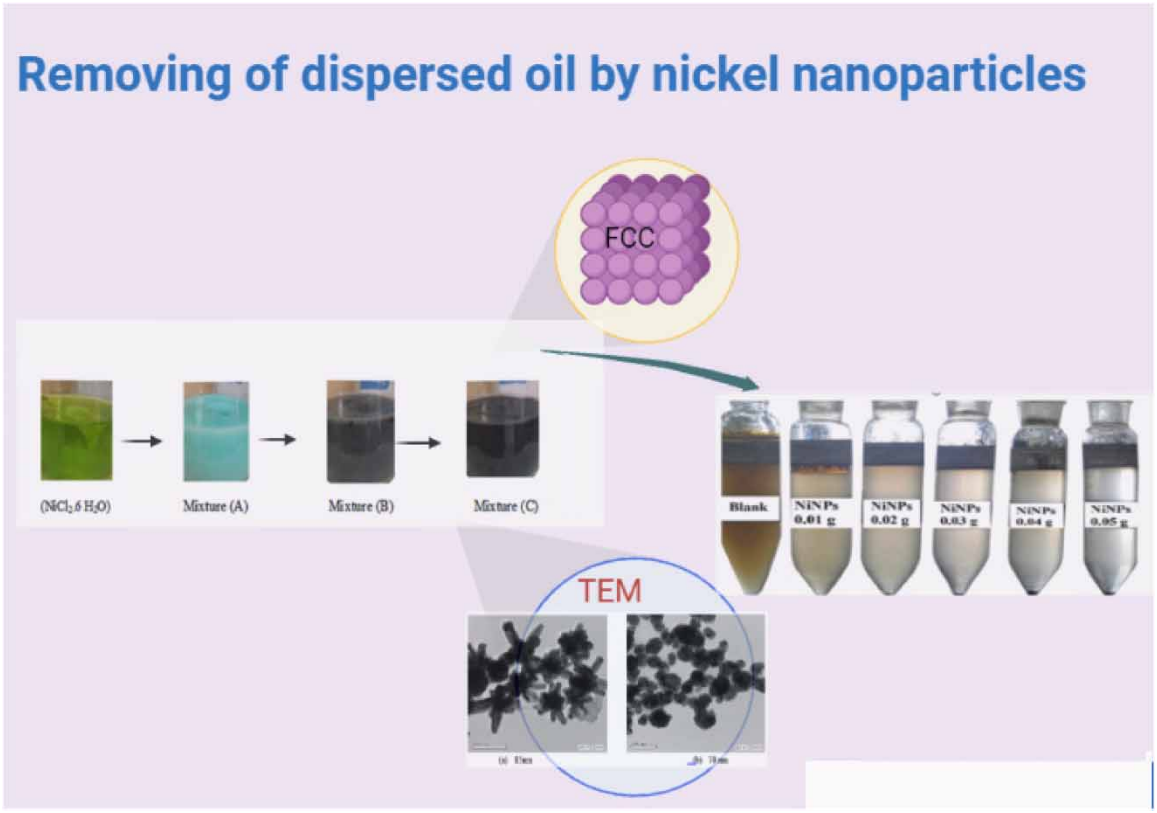

1. INTRODUCTION

Produced water is a byproduct of gas and oil production from both onshore and offshore wells (Spoonamore 2011; Alkhazraji & Alatabe 2021). Produced water is a mixture of oil, organic compounds, salts, heavy metals, radioactive elements, and dissolved oxygen. However, oil is dispersed in produced water during oil and gas operations. Produced water composed of different mixtures, BTEX (benzene, toluene, ethylbenzene, and xylene), classified as low molecular weight (382.59 g/mol). Another central combination of high molecular weight, less-soluble PAHs (polyaromatic hydrocarbons), and phenols (≈760 g/mol) were found. Experimental data showed that most oils in produced water are polar; however, dispersed oil is oil suspended in the aqueous phase (Igunnu & Chen 2014).

The amount of dispersed oil depends upon the density and viscosity of the oil, the water–oil tension interface, and the droplet history (Bretz *et al.* 1994). The ratio of oil to produced water varies widely from zero to more than 50% (2% oil and 98% water). The volume of produced water is directly proportional to the production of gas and oil (Henderson *et al.* 1999). Many techniques have been applied to separate and remove dispersed oil from produced water, such as biological, adsorption, membrane filtration, ionic surfactant, hydrocyclones, chemical oxidation, and electrochemical methods (Igunnu & Chen 2014). Nevertheless, there exist various limitations associated with these techniques, including high energy consumption during pressure plumb operations, the need for chemical usage in some cases, the potential requirement for pre- and post-treatment processes, and the overall costs being dependent on the volume of produced water (Pichtel 2016).

Nanoparticles offer several advantages as a potential technique for the treatment of produced water.

Enhanced contaminant removal: Nanoparticles have a high surface area-to-volume ratio, which allows for efficient adsorption and absorption of contaminants present in produced water and nanoparticles can be engineered and functionalized to target specific contaminants or classes of pollutants. They can be modified with different coatings, surface charges, or functional groups to enhance their affinity for particular pollutants (Yap *et al.* 2021).

The low-cost adsorbent powder is a valuable material for removing tiny oil droplets from produced water due to its large surface area (Ko *et al.* 2014). The magnetite and surface-coated magnetic nanoparticles attract

researchers for their applications in the separation and removal of oil from produced water (Igunnu & Chen 2014; Ko *et al.* 2014, 2017; Hosseini *et al.* 2018; Adewunmi *et al.* 2021).

Over recent decades, metallic nickel (Ni) and nickel oxide (NiO) nanoparticles have had various potential applications due to their remarkable properties, high ferromagnetic properties, high chemical stability, and coercive force. Therefore, they used adsorbents to purify water to remove heavy metals, anions, and dyes. They were also used as antimicrobial agents (Ravindhranath & Ramamoorty 2017; Jaji *et al.* 2020; Khoso *et al.* 2021). The magnetic nickel-ferrite nanoparticles (NFNs) are synthesized by co-precipitation and then used as adsorbents to remove heavy metals from wastewater (Khoso *et al.* 2021). The essential advantages and role of NiNPs as adsorbents for removing dispersed oil from produced water in oilfields (Jaji *et al.* 2020), top-down and bottom-up protocols prepare nickel nanoparticles (NiNPs). Therefore, NiNPs are fabricated by the bottom-up protocol by many methods such as sol-gel, spinning, chemical vapor deposition, pyrolysis, precipitation, and green methods. Trends in NiNP applications in fields such as biomedical, catalysis, supercapacitors, and dye-sensitized solar cells were explored.

Researchers recently synthesized a photocatalyst reactor for oil removal from produced water using zinc nanoparticles as a catalyst in batch and continuous systems (Alkhazraji & Alatabe 2021).

In Sudan oilfields, there is a problem with a tremendous amount of water accompanied by dispersed oil, contaminating the environment when discharged. Authors tried to find methods to remove dispersed oil from produced water. These methods include chemical and biological. To overcome this problem, the current study researchers synthesized NiNPs and then used them to treat spoiled oil in oilfield-produced water. To the best of our knowledge, this is the first time testing metallic nanoparticles for this purpose in Sudan.

2. MATERIALS AND METHODS

2.1. Sampling

Produced water samples were collected from Al-Fulah, an oil field in West Kordofan state in Sudan. In recent years, there has been a significant rise in the volume of produced water in Sudan's oil fields. This increase can be attributed to the growth in oil production and the aging of existing fields. Presently, approximately 1.2 million barrels per day of water are being produced in the national company (GNPOC) oil field in Sudan (Ahmed Khadam *et al.* 2009).

A colorimetric method was applied to determine oil concentration using DR6000 Spectrophotometer, HACH, USA. The calibration curve was constructed using a standard solution of 1000 mg L^{-1} of dispersed oil and *n*-hexane as an extraction solvent (Federation 1999). Quality control and assurance have been applied during the experiment.

2.2. Preparation of NiNPs

Nickel chloride hexahydrate ($NiCl_2{\cdot}6H_2O$), absolute ethanol 99%, sodium hydroxide (NaOH), and hydrazine monohydrate ($N_2H_4{\cdot}H_2O$) were involved in the synthesis of NiNPs.

NiNPs were prepared by adopting Zhiyu methods; a mixing of nickel chloride (3 g) was dissolved in ethanol. While sodium hydroxide (NaOH) was dissolved directly in absolute ethanol, two appropriate amounts of hydrazine monohydrate ($N_2H_4{\cdot}H_2O$) (5.4 and 8.2 g) were added. Meanwhile, the ratio between (N_2H_4/Ni^{2+} was 10 and 15). Mixture Ni-1 and mixture Ni-2, respectively, were indexed. The temperature was controlled to 60 °C with continuous stirring for 1 h and constant pH.

Nickel has been reduced from ions to atoms and directly accumulated to the nanoscale; the reaction can be addressed as follows (Wu & Chen 2003; Li *et al.* 2006):

$$2Ni^{2+} + N_2H_4 + 4OH^- \rightarrow \underset{\text{Nickel nanoparticles}}{2Ni} + N_2 + 4H_2O \quad (1)$$

Figure 1 illustrates the color transformation of the initial mixture, progressing from turquoise (Figure 1(a)) to gray after a 2-min interval (Figure 1(b)), and finally achieving a black color (Figure 1(c)). Following the duration of 1 h, the resulting precipitate was collected using a 0.45-μm filter after washed. It was then subjected to a series of washes using absolute ethanol, deionized water, and acetone 99%. Subsequently, the black precipitate was dried at room temperature and stored for further use in a sealed container for subsequent analysis. The reaction can be represented by Equation (1).

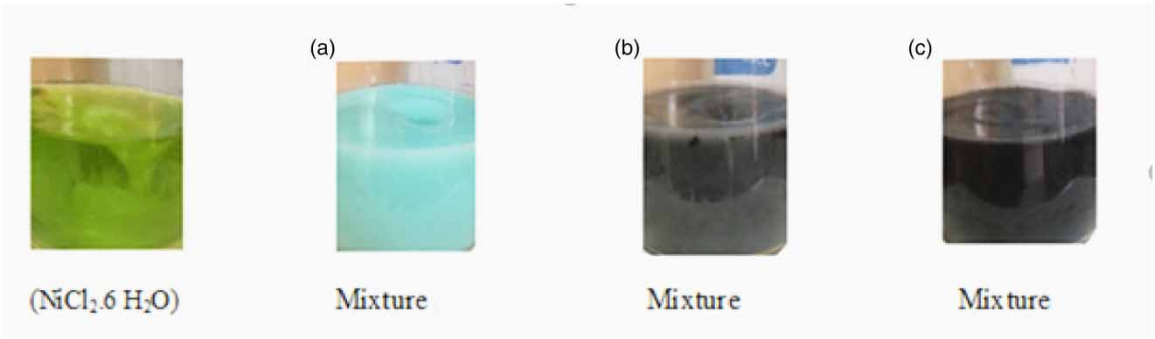

Figure 1 | Preparation of the nickel nanoparticles process. Mixture after 2 min (b) and mixture after 1 h (c).

2.3. Characterization procedure

The characterization of NiNPs was carried out using sophisticated techniques such as X-ray diffraction (XRD) and transmission electron microscope (TEM). The XRD analysis was performed by a PAN analytical 3 kW X'pert Powder XRD Multifunctional diffractometer with Cu Kα radiation source ($\lambda = 0.154$ nm). The crystalline phase and the average crystal size of metallic NiNPs were found by applying the Scherrer equation:

$$d = \frac{K\,\lambda}{\beta}\cos\theta \tag{2}$$

The particle size of NiNPs was determined by a TEM model H700H.

2.4. Batch adsorption experiment

Batch experiments (Ni-1 and Ni-2) were carried out to determine the adsorption isotherms of dispersed oil onto the adsorbents (NiNPs) as follows: Initial concentration (C_i) of dispersed oil in produced water sample was measured, shaken gently at a constant rate, and placed in the water bath at 60 °C. A series of different weights of the NiNPs ranging from 0.01, 0.02, 0.04, and 0.05 g were added to 100 ml of produced water. After equilibrium, the concentration of each sample was measured, and the logarithm of the adsorption capacity (q_e) and removal efficiency (%) at equilibrium were determined using Equations (3) and (4), respectively:

$$\text{Adsorption capacity}\, q_e = \frac{C_i - C_e}{W} \times V \tag{3}$$

$$\text{Removal efficiency}\,\% = \frac{C_i - C_e}{C_i} \times 100 \tag{4}$$

During experiments, q_e can be calculated in different forms, and it represents the adsorption capacity (mg g^{-1}), whereas C_i and C_e represent the initial and equilibrium concentrations (mg L^{-1}) of the adsorbate, and V and W stand for solution volume (L) and mass (g) of the adsorbent, respectively.

The main benefits of isotherms are considered equilibrium and interaction mechanisms between the adsorbent and the adsorbate at static temperature. Therefore, this equilibrium can be described by a set of models from one to five parameters. Langmuir and Freundlich cover two parameters (Liu *et al.* 2019; Jaji *et al.* 2020).

2.5. Adsorption and kinetics models

Langmuir isotherm considers some basic assumptions; the adsorption process between the adsorbent and the adsorbate is homogeneous, monolayer adsorption occurs onto the external surface, and the surface reaches a saturation point where the maximum adsorption of the surface will be achieved (Al-Ghouti & Da'ana 2020). The Langmuir equation is represented as follows:

$$q_e = q_{\max}\frac{K_L C_e}{1 + K_L C_e} \tag{5}$$

where $q_{\max}$ is the maximum adsorption capacity (mg g^{-1}), and K_L (L mg^{-1}) is Langmuir's isotherm constant,

which shows the binding affinity between dispersed oil and NiNPs. C_e and q_e are the liquid phase concentrations. The linear form of the Langmuir equation is:

$$\frac{1}{q_e} = \frac{1}{q_{\max} K_L C_e} + \frac{1}{q_{\max}} \tag{6}$$

In the linear equation, $1/q_e$ vs. $1/C_e$ were plotted as a mathematics function, therefore, K_L and $q_{\max}$ were calculated directly from the value of slope and intercept, respectively.

While the separation factor (R_L) is calculated by using Equation (7):

$$R_L = \frac{1}{1 + C_i \times K_L} \tag{7}$$

where R_L is the dimensionless Langmuir constant which indicates the adsorption possibility either favorable ($0 < R_L > 1$), unfavorable ($R_L > 1$), linear ($R_L = 1$), or irreversible ($R_L = 0$) (Ayub *et al.* 2020).

Freundlich isotherm includes the following assumptions: Heterogeneous distribution of active site and energies and present multilayer surface between adsorbents and adsorbate. Freundlich's isotherm equation is:

$$q_e = K_f C_e^{\frac{1}{n}} \tag{8}$$

The linear form of Freundlich's isotherm is:

$$\text{Log}\, q_e = \text{Log}\, K_f + \frac{1}{n}\, \text{Log}\, C_e \tag{9}$$

Freundlich constant and K_f and n values can be obtained from the slope and intercept of plotting Log q_e vs. Log C_e in the linear form of the equation.

Therefore, K_f is Freundlich's constant used to measure the adsorption capacity, and $1/n$ is the adsorption intensity. The value of $1/n$ demonstrates the adsorption process is either favorable ($0.1 < 1/n < 0.5$) or unfavorable ($1/n > 2$) (Ayawei *et al.* 2017).

In addition, the pseudo-first-order and pseudo-second-order have been applied to determine the time of oil adsorption on NiNPs and enhance experimental data to obtain the best results. To describe the mechanism of the kinetics of adsorption of dispersed oil on NiNPs, two models have been applied to Equations (10) and (11) in Table 1 (Li *et al.* 2012).

Table 1 | Kinetics models

Kinetic models	Equation	Plot	Constants and parameters	Eq. no	Ref
Pseudo-first-order	$\ln(q_e - q_t) = \ln(q_e) - K_1 t$	$\ln(q_e - q_t) Vs t$	$q_e = \exp(\text{intercept})$ $K_1 = -(\text{slope})$	(10)	Dehmani & Abouarnadasse (2020)
Pseudo-second-order	$\frac{t}{q_t} = \frac{1}{q_t^2} + \frac{1}{q_t} t$	$\frac{t}{q_t}\ Vs\ t$	$q_e = \frac{1}{\text{slope}}$ $K_2 = \frac{\text{slope}^2}{\text{intercept}}$	(11)	Dehmani & Abouarnadasse (2020)

3. RESULTS AND DISCUSSION

3.1. Characterization results

The XRD results showed that NiNPs formed by the reduction of Ni^{2+} with hydrazine were crystalline, which is identical to recorded results found in the literature (Wu & Chen 2003; Khoso *et al.* 2021). XRD data in Figure 2 showed that Ni-1 displayed three main distinct diffraction peaks recorded at 44.57°, 51.9°, and 76.4°. Therefore,

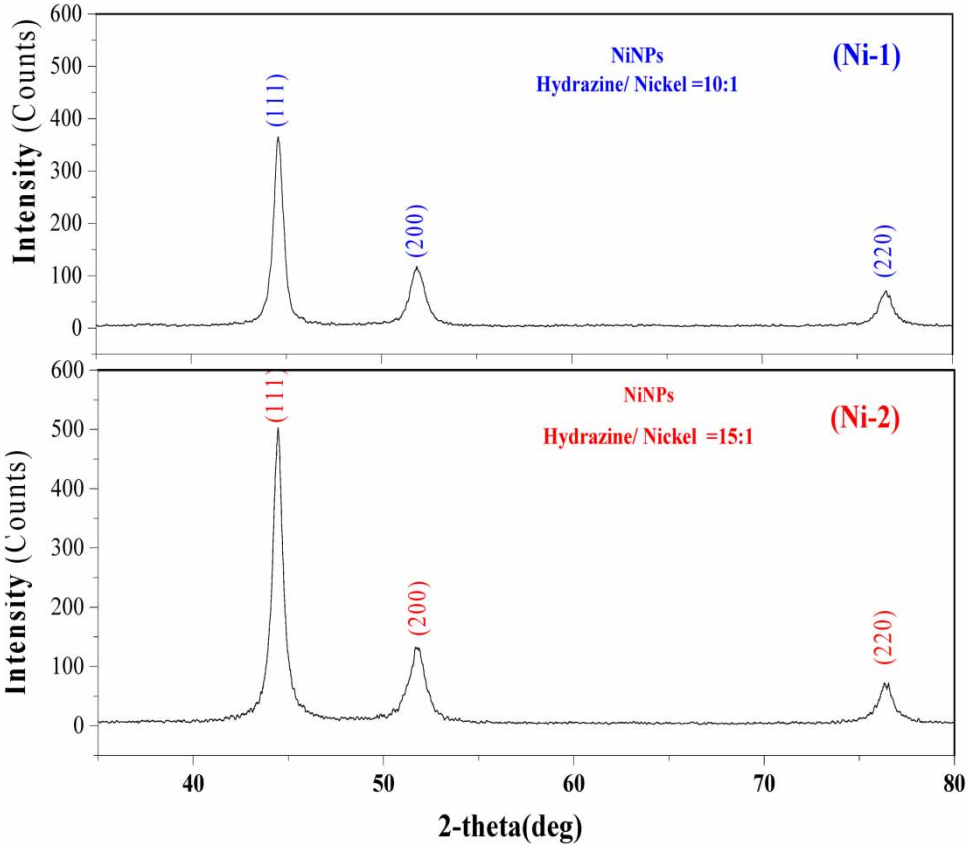

Figure 2 | XRD patterns of Ni-1 and Ni-2.

their corresponding miller indices are Ni (111), Ni (200), and Ni (220), which demonstrate face-centered cubic (FCC), while XRD data of Ni-2 displays three distinct diffraction peaks at 44.52°, 51.70°, and 76.39°. The highest pick was recorded at 44.42° at 2θ with miller indices Ni (111), Ni (200), and Ni (220). This result indicates that NiNPs have been reduced from ions to nanoscale successfully.

Moreover, the average particle size determined by the Debye-Scherrer equation was found 12 nm for both ratios.

The TEM monograph image and size distribution of NiNPs are shown in Figure 3(a) and 3(b) for both samples. The main particle of Ni-1 indicates a fine star structure with a mean diameter of 85 nm which is attributed to plans FCC NiNPs Ni (111) plan. Nevertheless, in low concentration Ni-2, the morphology changed to monodispersed spherical particles with an average size close to 70 nm. As the ratio of N_2H_2/Ni^{2+} increases, the mean

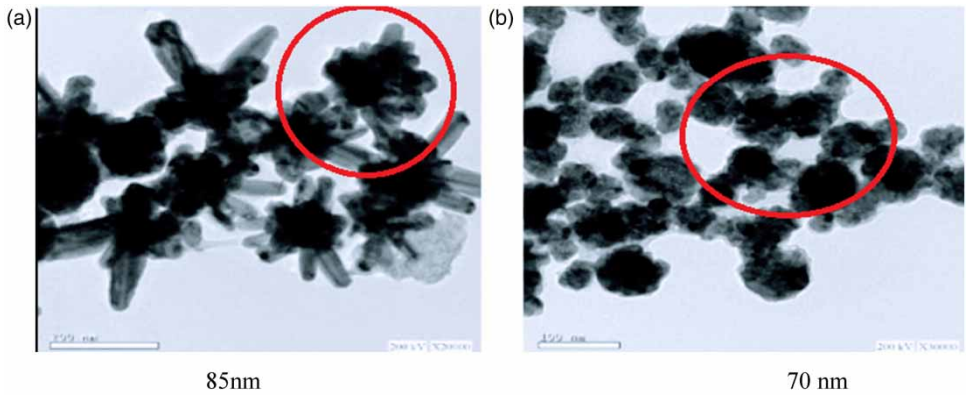

Figure 3 | Ni-1 and Ni-2 TEM images (a) 85 nm and (b) 70 nm.

diameter decreases, and hence, the morphologies of NiNPs changed from star-like to spherical shape. It can be explained by the influence of the reduction rate on nucleation. Moreover, when most nuclei form, they almost simultaneously grow at the same rate, and the resultant nanoparticles will be monodispersed. At lower hydrazine concentrations, the formation of larger particles with star-like shapes was attributed to the slow reduction rate of nickel chloride, and only a few nuclei formed at the beginning of the reduction reaction. While, with the increase in hydrazine concentration, the reduction rate favored the generation of much more nuclei and the formation of smaller NiNPs (Wu & Chen 2003; Wu *et al.* 2010; Zhu *et al.* 2019; Figure 4; Table 2).

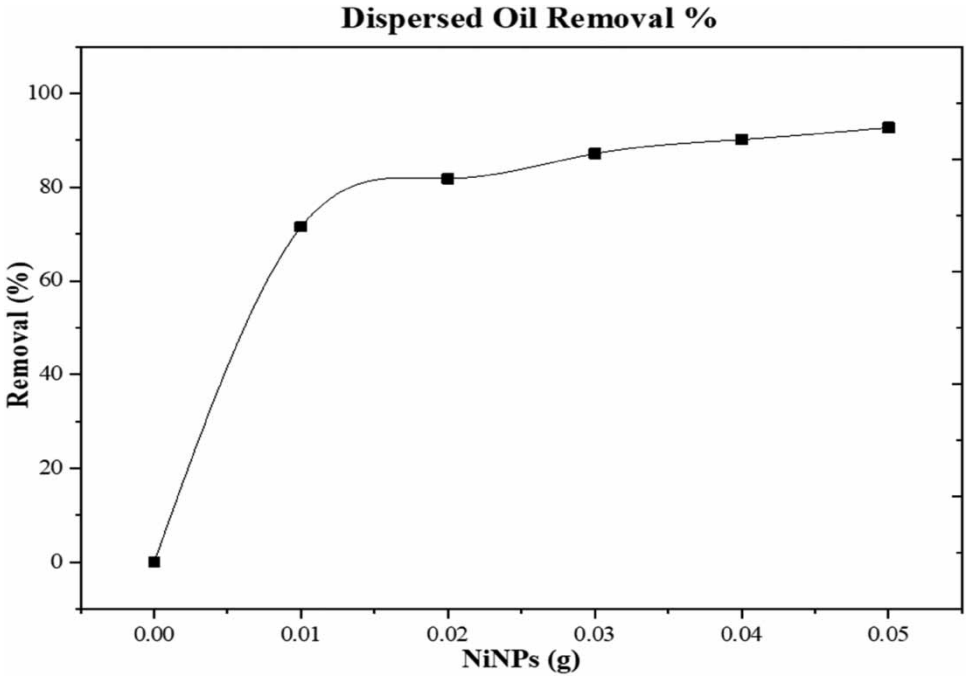

Figure 4 | Removal of dispersed oil from produced water percentage.

Table 2 | Physical properties of produced water samples

Parameters	Maximum value	Minimum value
pH	8 at T = 26.5 °C	7.4 at T = 26.5 °C
Oil and grease (mg L^{-1})	300	200
TDS (mg L^{-1})	1,217	950
Conductivity (μS/cm)	4,200	3,800
Total oil (IR, mg L^{-1})	380	59

3.2. Adsorption and kinetics evaluation

Langmuir–Freundlich isotherm includes the knowledge of the adsorption of heterogeneous surfaces. It describes the adsorption energy distribution onto the adsorbent's heterogeneous surface. The adsorption isotherm provides valuable information about adsorption capacity, binding affinity, and the surface properties of the NiNPs so that the binding mechanism of adsorbate can be understood. Two theoretical models, Langmuir and Freundlich's isotherms, were used to examine the adsorption behavior of NiNPs for dispersed oil uptake into NiNP surfaces, as shown in Figures 5 and 6. Langmuir's isotherm describes the monolayer adsorption of dispersed oil adsorbate onto the NiNP surface, having a finite number of adsorption sites. Freundlich's isotherm supports that adsorption occurs on the heterogeneous surface of the adsorbent. At low adsorbate concentration, this model becomes the

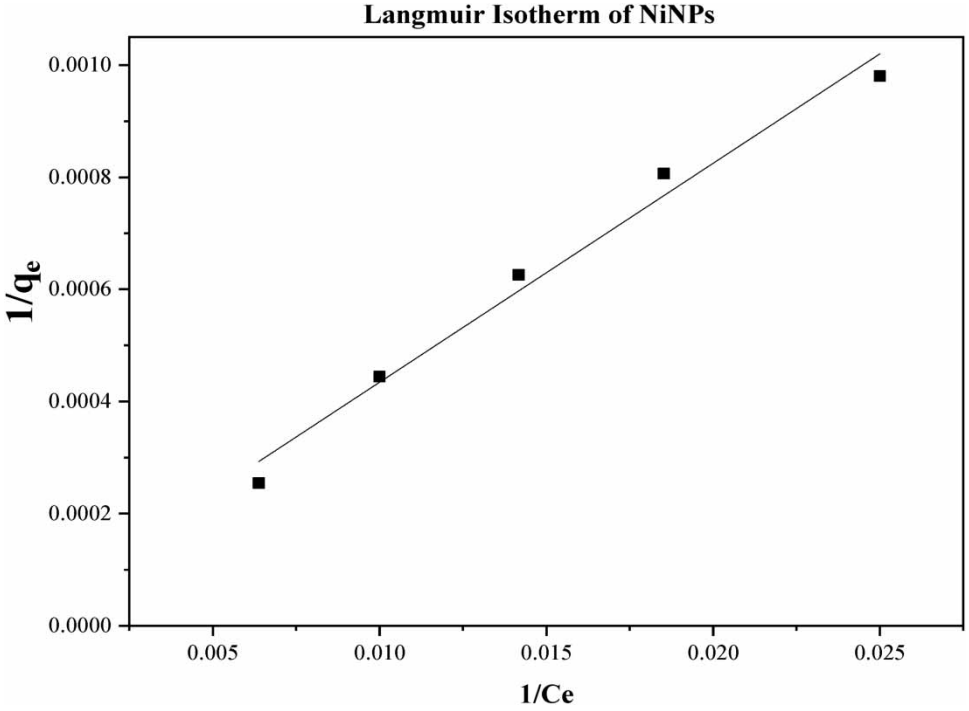

Figure 5 | Langmuir's isotherm plots for the adsorption of dispersed oil onto NiNPs.

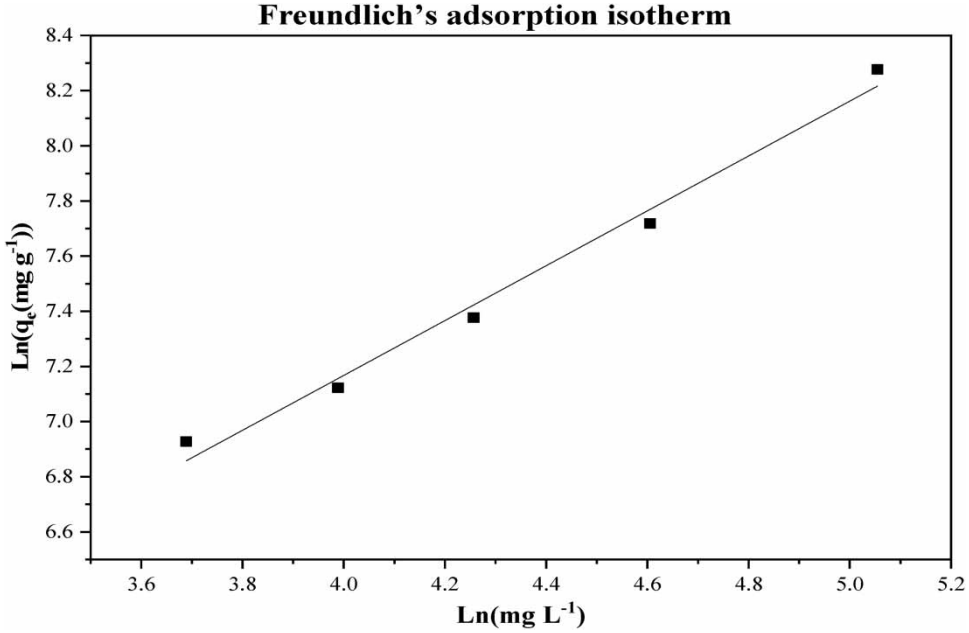

Figure 6 | Freundlich's isotherm plots for the adsorption of dispersed oil onto NiNPs.

Freundlich isotherm model, while at high adsorbate concentration, it becomes the Langmuir isotherm (Ayawei *et al.* 2017). Table 3 shows adsorption information.

The removal fits well with Freundlich's isotherm since the value of the linear regression coefficient ($R^2 =$ 0.98314) is higher than Langmuir's isotherm ($R^2 = 0.9775$). The results illustrate that dispersed oil adsorbate forms a physical adsorption monomolecular layer into the internal surface of NiNPs.

Table 3 | Freundlich and Langmuir constants for adsorption of dispersed oil using nickel nanoparticles

W (g)	C_i (mg L^{-1})	C_e (mg L^{-1})	q_e (mg g^{-1})	$1/C_e$	ln C_e	$1/q_e$	ln q_e	Removal (%)
0.01	550	157	3932	0.0064	5.0547	2.5×10^{-4}	8.28	71.5
0.02	550	100	2250	0.0100	4.6052	4.4×10^{-4}	7.72	81.8
0.03	550	71	1598	0.0142	4.2569	6.3×10^{-4}	7.38	87.2
0.04	550	54	1240	0.0185	3.9890	8.1×10^{-4}	7.12	90.2
0.05	550	40	1020	0.0250	3.6889	9.8×10^{-4}	6.92	92.7

The maximum adsorption capacity of NiNPs for dispersed oil was 22,841 mg g^{-1}. The value of the separation factor (R_L) for NiNPs is less than one (0.670), which favors the adsorption phenomenon. The data in Table 4 demonstrate Langmuir isotherm parameters information.

Table 4 | Langmuir's isotherm parameters for the removal of dispersed oil by NiNPs

Intercept	Slope	q_{max} (mg g^{-1})	K_L (L mg^{-1})	R_L	R^2
0.000044	0.03905	22,841	0.001121	0.670	0.9775

Kinetics models pseudo first and second orders were applied to perform the concentration change per time. The ability of NiNPs to remove dispersed oil from produced water was governed by q_e (Figure 7). The value shifted when powder doses increased to 3,932, 2,250, 1,598, 1,240, and 1,020 mg g^{-1}, respectively. The rise of NiNP doses does not restrict the adsorption process q_e. The pseudo-first and second kinetics order values were 14.04 and 833.3 mg g^{-1}, respectively, indicating that the dispersed oil fit well with the pseudo-second-order reaction. Correlation factor R^2 is used to fit the best kinetics model in Table 5. So R^2 of the second order is 0.998, proving that the experimental results of adsorption of dispersed oil on the adsorbent are well described by the second-order kinetic. The K_2 value is very lower than 1.93×10^{-3}, illustrating that the adsorption was rapid. Consequently, Dehmani and his co-workers studied the ability of nickel oxide nanoparticles to remove phenol at different temperatures. Thus, the adsorption amount increased when the temperature was raised. According to calculated correlation coefficients, the adsorption kinetics of phenol on nickel oxide nanoparticles fit very well to pseudo-second-order (Pirmoradi *et al.* 2017; Dehmani & Abouarnadasse 2020; Figures 8 and 9).

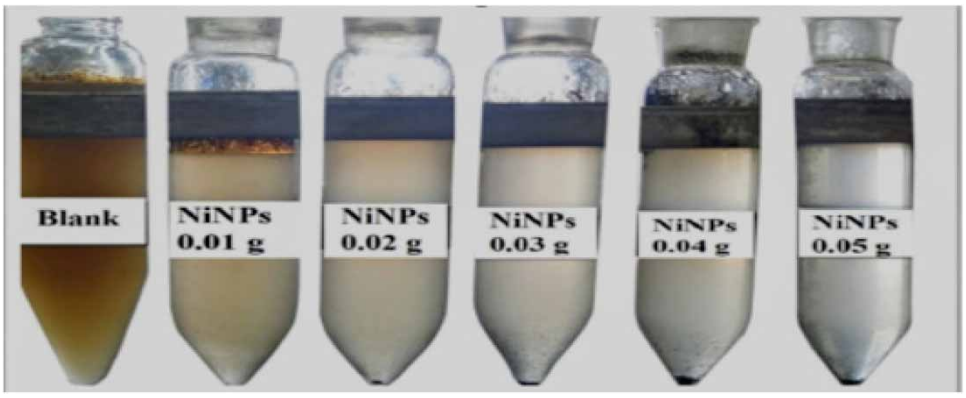

Figure 7 | The effect of NiNP doses on dispersed oil removal.

Oil dispersed removal from produced water quickly by magnetic nanoparticles as recorded in literature because of external magnetic field force. Therefore, it successfully separates oil droplets from attached water (Ko *et al.* 2014). Figure 4 shows the removal percentage vs. NiNP doses; it can be noticed that there are two adsorption processes. In the first step, the interaction between dispersed oil and the side surface of NiNPs

Table 5 | Kinetic parameters for removal of dispersed oil using nickel nanoparticles

	Intercept	Slope	q_e (mg g^{-1})	*K*-value	R^2
Pseudo-first-order	2.64202	0.07329	14.04	0.0014658	0.238
Pseudo-second-order	7.45E-04	0.0012	833.33	1.93×10^{-3}	0.998

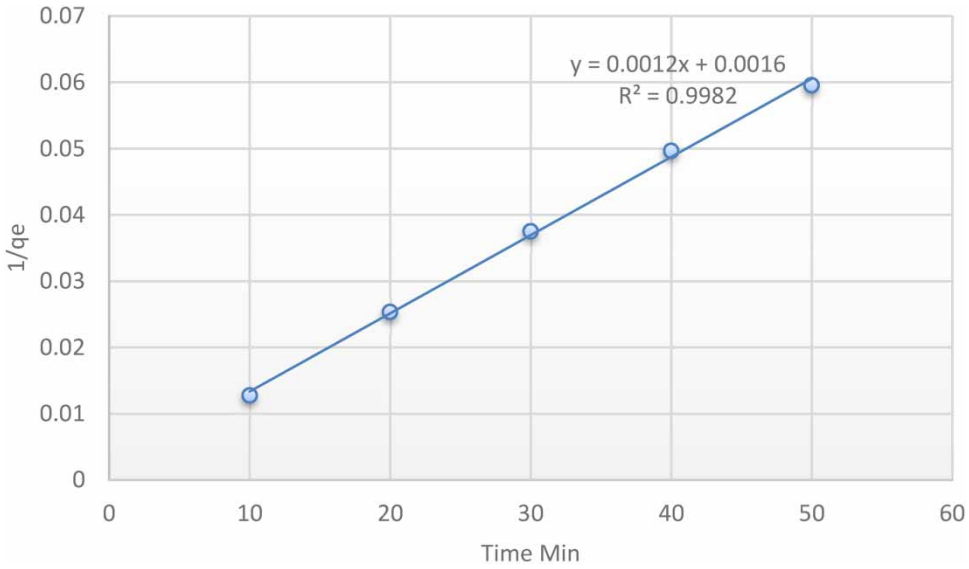

Figure 8 | Pseudo-second model.

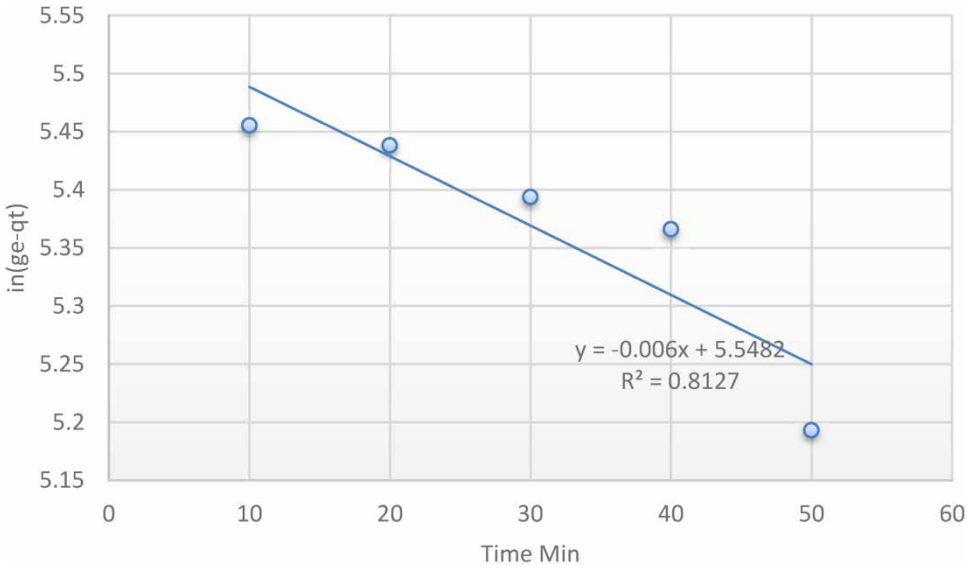

Figure 9 | Pseudo-first model.

before saturated, while in the second step, dispersed oil molecules saturated the pore size of the NiNPs, and adsorption was reduced due to weak concentration (Gerçel & Gerçel 2007; Bhatnagar *et al.* 2010).

Positively magnetic nanoparticles crafted by the amine functional group showed high removal of oil from emulsion solution found at 99.5, 97.9, and 96.4%, respectively, by electrostatic forces. Positively magnetic nanoparticles have destroyed the stabilization energy barrier between oil drops, and it separated from the water easily (Ko *et al.* 2017).

Meanwhile, nickel is essential to transition elements, its magnetic properties higher than the other elements rather than the iron family. The saturated magnetization (*Ms*) of NiNPs was estimated to be between 50 and 60 emu g^{-1} (Hwang *et al.* 1997; Simonsen *et al.* 2018). Different weights of NiNPs showed a high ability to remove dispersed oil from produced water. The removal percentage was 98% (40 mg L^{-1}). Figure 4 represents the relationship between NiNP doses and removal percentage.

4. CONCLUSIONS

A new nickel-nanoparticle adsorbent was synthesized through a thermal decomposition process. Hydrazine and sodium hydroxide were employed as reducing agents and a solvent, respectively. When applied to treat oilfield-produced water, the findings indicated that the resulting water was effectively purified and suitable for agricultural reuse. The evaluation of fit quality and adsorption performance often involves the use of linear regression analysis due to its broad applicability in different adsorption data. Furthermore, several researchers have extensively employed nonlinear regression analysis to bridge the gap between predicted and experimental data. Consequently, it is crucial to determine and clarify the utility of both linear and nonlinear regression analysis in various adsorption systems.

DATA AVAILABILITY STATEMENT

All relevant data are included in the paper or its Supplementary Information.

CONFLICT OF INTEREST

The authors declare there is no conflict.

REFERENCES

Adewunmi, A. A., Kamal, M. S. & Solling, T. I. 2021 Application of magnetic nanoparticles in demulsification: a review on synthesis, performance, recyclability, and challenges. *Journal of Petroleum Science and Engineering* **196**. https://doi.org/10.1016/j.petrol.2020.107680.

Ahmed Khadam, M., Ahmed Agab, M. & Saad, G. 2009 Biological method for treatment of petroleum produced water oil content in Sudan. *Sudan Engineering Society Journal* **55**(52). https://www.researchgate.net/publication/281004364_BIOLOGICAL_METHOD_FOR_TREATMENT_OF_PETROLEUM_PRODUCED_WATER_OIL_CONTENT_IN_SUDAN.

Al-Ghouti, M. A. & Da'ana, D. A. 2020 Guidelines for the use and interpretation of adsorption isotherm models: a review. *Journal of Hazardous Materials* **393**, 122383. https://doi.org/10.1016/j.jhazmat.2020.122383.

Alkhazraji, H. A. & Alatabe, M. J. 2021 Oil recovery from oilfield produced water using zinc oxide nanoparticle as catalyst in batch and continuous system. *Journal of Ecological Engineering* **22**(8), 278–286. https://doi.org/10.12911/22998993/140281.

Ayawei, N., Ebelegi, A. N. & Wankasi, D. 2017 Modelling and interpretation of adsorption isotherms. *Journal of Chemistry*. https://doi.org/10.1155/2017/3039817.

Ayub, A., Raza, Z. A., Majeed, M. I., Tariq, M. R. & Irfan, A. 2020 Development of sustainable magnetic chitosan biosorbent beads for kinetic remediation of arsenic contaminated water. *International Journal of Biological Macromolecules* **163**, 603–617. https://doi.org/10.1016/j.ijbiomac.2020.06.287.

Bhatnagar, A., Minocha, A. K. & Sillanpää, M. 2010 Adsorptive removal of cobalt from aqueous solution by utilizing lemon peel as biosorbent. *Biochemical Engineering Journal* **48**(2), 181–186. https://doi.org/10.1016/j.bej.2009.10.005.

Bretz, R. E., Martin, F. D. & Russell, C. 1994 Produced water: technological/environmental issues and solutions. *Journal of Environmental Quality* **23**(2), 391–391. https://doi.org/10.2134/jeq1994.00472425002300020034x.

Dehmani, Y. & Abouarnadasse, S. 2020 Study of the adsorbent properties of nickel oxide for phenol depollution. *Arabian Journal of Chemistry* **13**(5), 5312–5325. https://doi.org/10.1016/j.arabjc.2020.03.010.

Federation, W. E. 1999 Standard methods for the examination of water and wastewater. *Public Health* **51**(1), 940. https://doi.org/10.2105/AJPH.51.6.940-a.

Gerçel, Ö. & Gerçel, H. F. 2007 Adsorption of lead(II) ions from aqueous solutions by activated carbon prepared from biomass plant material of *Euphorbia rigida*. *Chemical Engineering Journal* **132**(1–3), 289–297. https://doi.org/10.1016/j.cej.2007.01.010.

Henderson, S. B., Grigson, S. J. W., Johnson, P. & Roddie, B. D. 1999 Potential impact of production chemicals on the toxicity of produced water discharges from North Sea oil platforms. *Marine Pollution Bulletin* **38**(12), 1141–1151. https://doi.org/10.1016/S0025-326X(99)00144-7.

Hosseini, S. S., Fakharian Torbati, S., Alaei Shahmirzadi, M. A. & Tavangar, T. 2018 Fabrication, characterization, and performance evaluation of polyethersulfone/TiO_2 nanocomposite ultrafiltration membranes for produced water treatment. *Polymers for Advanced Technologies* **29**(10), 2619–2631. https://doi.org/10.1002/pat.4376.

Hwang, J. H., Dravid, V. P., Teng, M. H., Host, J. J., Elliott, B. R., Johnson, D. L. & Mason, T. O. 1997 Magnetic properties of graphitically encapsulated nickel nanocrystals. *Journal of Materials Research* **12**(4), 1076–1082. https://doi.org/10.1557/JMR.1997.0150.

Igunnu, E. T. & Chen, G. Z. 2014 Produced water treatment technologies. *International Journal of Low-Carbon Technologies* **9**(3), 157–177. https://doi.org/10.1093/ijlct/cts049.

Jaji, N. D., Lee, H. L., Hussin, M. H., Akil, H. M., Zakaria, M. R. & Othman, M. B. H. 2020 Advanced nickel nanoparticles technology: from synthesis to applications. *Nanotechnology Reviews* **9**(1), 1456–1480. https://doi.org/10.1515/ntrev-2020-0109.

Khoso, W. A., Haleem, N., Baig, M. A. & Jamal, Y. 2021 Synthesis, characterization and heavy metal removal efficiency of nickel ferrite nanoparticles (NFNs). *Scientific Reports* **11**(1), 1–10. https://doi.org/10.1038/s41598-021-83363-1.

Ko, S., Prigiobbe, V., Huh, C., Bryant, S., Bennetzen, M. V. & Mogensen, K. 2014 Accelerated oil droplet separation from produced water using magnetic nanoparticles. Proceedings – SPE Annual Technical Conference and Exhibition, Vol. 5, pp. 3408–3421. https://doi.org/10.2118/170828-ms.

Ko, S., Kim, E. S., Park, S., Daigle, H., Milner, T. E., Huh, C., Bennetzen, M. V. & Geremia, G. A. 2017 Amine functionalized magnetic nanoparticles for removal of oil droplets from produced water and accelerated magnetic separation. *Journal of Nanoparticle Research* **19**(4). https://doi.org/10.1007/s11051-017-3826-6.

Li, Z., Han, C. & Shen, J. 2006 Reduction of Ni^{2+} by hydrazine in solution for the preparation of nickel nano-particles. *Journal of Materials Science* **41**(11), 3473–3480. https://doi.org/10.1007/s10853-005-5874-z.

Li, Y., Du, Q., Liu, T., Sun, J., Jiao, Y., Xia, Y., Xia, L., Wang, Z., Zhang, W., Wang, K., Zhu, H. & Wu, D. 2012 Equilibrium, kinetic and thermodynamic studies on the adsorption of phenol onto graphene. *Materials Research Bulletin* **47**(8), 1898–1904. https://doi.org/10.1016/j.materresbull.2012.04.021.

Liu, L., Luo, X. B., Ding, L. & Luo, S. L. 2019 Application of Nanotechnology in the Removal of Heavy Metal From Water. In: *Nanomaterials for the Removal of Pollutants and Resource Reutilization*. (pp. 83–147). Elsevier Inc., https://doi.org/10.1016/B978-0-12-814837-2.00004-4.

Pichtel, J. 2016 Oil and gas production wastewater: soil contamination and pollution prevention. *Applied and Environmental Soil Science* **2016**. https://doi.org/10.1155/2016/2707989.

Pirmoradi, M., Hashemian, S. & Shayesteh, M. R. 2017 Kinetics and thermodynamics of cyanide removal by ZnO@NiO nanocrystals. *Transactions of Nonferrous Metals Society of China (English Edition)* **27**(6), 1394–1403. https://doi.org/10.1016/S1003-6326(17)60160-2.

Ravindhranath, K. & Ramamoorty, M. 2017 Nickel based nanoparticles as adsorbents in water purification methods – a review. *Oriental Journal of Chemistry* **33**(4), 1603–16013. https://doi.org/10.13005/ojc/330403.

Simonsen, G., Strand, M. & Øye, G. 2018 Potential applications of magnetic nanoparticles within separation in the petroleum industry. *Journal of Petroleum Science and Engineering* **165**, 488–495. https://doi.org/10.1016/j.petrol.2018.02.048.

Spoonamore, S., 2011 Produced water. In: *Filtration and Separation in the New Energy Era-2011 AFS Fall Topical Conference* (Neff, J. M., Lee, K. & DeBlois, E. M., eds). p. 52. https://doi.org/10.1016/b978-008043716-3/50002-6.

Wu, S.-H. & Chen, D.-H. 2003 Synthesis and characterization of nickel nanoparticles by hydrazine reduction in ethylene glycol. *Journal of Colloid and Interface Science* **259**(2), 282–286. https://doi.org/10.1016/S0021-9797(02)00135-2.

Wu, Z. G., Munoz, M. & Montero, O. 2010 The synthesis of nickel nanoparticles by hydrazine reduction. *Advanced Powder Technology* **21**(2), 165–168. https://doi.org/10.1016/j.apt.2009.10.012.

Yap, P. L., Nine, M. J., Hassan, K., Tung, T. T., Tran, D. N. H. & Losic, D. 2021 Graphene-based sorbents for multipollutants removal in water: a review of recent progress. *Advanced Functional Materials* **31**(9). Wiley-VCH Verlag. https://doi.org/10.1002/adfm.202007356.

Zhu, L., Cui, J., Zhang, H., Ruan, L., Ma, N., Zou, L., Deng, T., Chen, B. H. & Xiao, Q. 2019 Room-temperature morphology-controlled synthesis of nickel and catalytic properties of corresponding Ru/Ni catalysts. *ChemCatChem* **11**(13), 3109–3116. https://doi.org/10.1002/cctc.201900565.

First received 8 March 2023; accepted in revised form 31 August 2023. Available online 14 September 2023